J. Theo. and Appl. Fluid Mech.
Vol. 1, No. 3, December 1996, pp. 154-170

THE EFFECT OF INERTIA ON THE STABILITY OF CONVECTION IN A POROUS LAYER HEATED FROM BELOW

D.A.S. REES
School of Mechanical Engineering
University of Bath
Claverton Down
Bath. BA2 7AY, U.K.

(Received 27 July 1995; accepted in revised form 12 June 1996).

Abstract In this paper we consider the modification to the weakly nonlinear stability of convection in a porous layer heated from below which is brought about by the presence of fluid inertia as modelled by the so-called Forchheimer term. The overall aim of this paper is to determine both qualitative and quantitative criteria which may be used in careful experimental work to validate or otherwise the Forchheimer terms as a suitable representation of the presence of microscopic inertia in porous medium flows. Using the form of analysis introduced by Newell and Whitehead (1969) for the Bénard problem, we consider the stability of steady roll convection with respect to the Eckhaus, zigzag and cross–roll instability mechanisms. It is found that all three curves are modified when inertia effects are present. In particular, rolls with a wavenumber less than the critical value are no longer unconditionally unstable. The Eckhaus and zigzag stability bounds are less restrictive than for the zero–inertia case, but the opposite is true for the cross–roll instability. In some instances the Eckhaus instability is more dangerous than the zigzag instability. Detailed results are presented and the implications given for the range of possible flows and the realised rates of heat transfer.

1. Introduction

We consider the stability of convection in a horizontal layer of saturated porous medium which is heated uniformly from below. This is the porous medium analogue of the classical Bénard problem and it was first studied by Lapwood (1948) and Horton and Rogers (1945). These authors considered the linear stability of the basic state which consists of a linear temperature drop across the layer from the lower surface to the upper surface, and no flow. Thus a neutral curve was obtained relating the Darcy–Rayleigh number to the wavenumber of the cellular motion. Although rolls of any wavenumber are mathematically realisable as long as the Darcy–Rayleigh number is sufficiently high, they are not necessarily physically realisable if the layer has a very large horizontal dimension. A similar situation pertains for the Bénard problem where the range of stable wavenumbers was obtained by both Schlüter, Lortz and Busse (1965) and Newell and Whitehead (1969). Analyses similar to that of Newell and Whitehead were given by Rees and Riley (1989a,b) for the porous Bénard problem, although the main aim of those papers was the investigation of the effects of small-amplitude thermal modulations on the heated surfaces. These analyses are of vital importance since the delineation of the range of stable wavenumbers gives bounds for the realisable rates of heat transfer through the layer. In addition, the qualitative nature of the weakly nonlinear results often carry well into the strongly nonlinear regime even if the quantitative results are at variance.

In recent years many studies have appeared which deal with the effects of imperfections of various types on convection in porous layers. For example, Kvernvold and Tyvand (1980) looked at thermal dispersion, McKibbin and O'Sullivan (1980, 1981) and Rees and Riley (1990) considered a layered medium, and Rees and Riley (1989a,b) and Rees (1990) considered either thermal modulations or boundary undulations. In this paper we have been motivated by the studies of Nield and Joseph (1985) who considered the effect of fluid inertia, and of He and Georgiadis (1990) who considered the combined effects of inertia, thermal dispersion and internal heating. The particular inertia terms considered in these papers are known as the quadratic drag, or Forchheimer terms; these were first introduced by Forchheimer (1901) in the form of a one-dimensional equation, but many later authors have extended this to two and three dimensions in a straightforward way allowing for frame-invariance. The detailed theoretical reasons behind the introduction of the quadratic inertia term have been the subject of some debate in the fairly recent literature. For example, Hassanizadeh & Gray (1987) argue that a nonlinear relationship between the applied pressure head and the resulting macroscopic flow arises from microscopic drag forces. On the other hand, Ruth & Ma (1992), demonstrate the intricate dependence of the macroscopic flow on the detailed micro-structure of the medium, and hence, they conclude, microscopic inertia forces are responsible for the loss of linearity in Darcy's law. A more recent paper by Rasoloarijoana & Auriault (1994) has made a case for using a cubic law instead of a quadratic law. However, it is not the aim of this paper to justify the use of the quadratic law, but to consider in detail the implications of assuming its validity in the case of the porous medium analogue of the Bénard problem.

Nield & Joseph (1985) found that the usual pitchfork bifurcation, which occurs at onset of convection in the Darcy–Bénard problem, is replaced by a degenerate structure consisting of two straight lines with a sharp "nose" at the point of onset of convection. When thermal dispersion and internal heating are also included in the modelling of the medium, the straight lines become disjointed and no longer branch away from the no-flow curve at the same value of the Darcy–Rayleigh number (He & Georgiadis 1990). Both the papers cited in this paragraph were concerned with cases where inertia has a strong effect

and therefore the weakly nonlinear analysis needed only to proceed as far as the second order to give useful results. In the present paper we revisit this problem but in a simplified form: we neglect thermal dispersion effects and assume that internal heating is absent. Further, we shall assume that inertia has only a weak effect — it is this weak presence of inertia which we can regard as an imperfection. Although this seems like a very considerable simplification of the overall problem, such a simplification allows us to describe clearly the transition from the Darcy–Bénard case, where inertia is completely absent, to that given by He and Georgiadis and by Nield and Joseph where inertia dominates entirely. By so doing we are extending the type of analysis undertaken by these authors since a stability analysis was outside the scope of their papers.

2. Governing equations

The nondimensional equations governing free convection flow in a porous medium are given by

$$u_x + v_y + w_z = 0, \tag{1a}$$

$$u(1+Gq) = p_x, \tag{1b}$$

$$v(1+Gq) = -p_y + R\theta, \tag{1c}$$

$$w(1+Gq) = -p_z, \tag{1d}$$

$$\theta_t + u\theta_x + v\theta_y + w\theta_z = \theta_{xx} + \theta_{yy} + \theta_{zz}, \tag{1e}$$

where $R = \rho g \hat{\beta} d K \Delta T/\mu\kappa$ is the Darcy–Rayleigh number based on ρ, the reference density; g, gravity; $\hat{\beta}$, the coefficient of cubical expansion; d, the depth of the layer; K, the permeability of the medium; ΔT, the temperature drop across the layer; μ, the fluid viscosity; and κ, the thermal diffusivity. In equations (1b), (1c) and (1d) the fluid flux speed, q, is given by

$$q^2 = u^2 + v^2 + w^2, \tag{2}$$

where q is taken to be positive, and the inertia parameter, G, is given by

$$G = \frac{\tilde{K}\rho\kappa}{\mu d}. \tag{3}$$

By way of illustration, values of K and the material parameter, $\tilde{K}$, are given by Ergun's experimental relations, (cf. Ergun (1952))

$$K = \frac{L^2\Phi^3}{150(1-\Phi)^2}, \qquad \tilde{K} = \frac{1.75L}{150(1-\Phi)}, \tag{4}$$

where L is a characteristic particle or pore diameter and Φ denotes the porosity of the medium. In deriving equations (1) the Boussinesq approximation has been invoked, and it is assumed that the velocity field adjusts instantaneously to changes in the pressure and temperature.

For three–dimensional flows equations (1) must be used, but when the flow is two–dimensional a streamfunction/temperature formulation may be introduced by setting

$$u = \psi_y, \qquad v = -\psi_x \qquad \text{and} \qquad w = 0 \tag{5}$$

in (1). The most convenient form of the resulting equations is

$$(1 + Gq)(\psi_{xx} + \psi_{yy}) + G(\psi_x q_x + \psi_y q_y) = R\theta_x, \tag{6a}$$

$$\theta_t + \psi_x \theta_y - \psi_y \theta_x = \theta_{xx} + \theta_{yy}. \tag{6b}$$

Equations (1) and (6) are to be solved subject to the boundary conditions,

$$y = 0: \qquad v = 0, \quad \psi = 0, \quad \theta = 1, \tag{7a}$$

$$y = 1: \qquad v = 0, \quad \psi = 0, \quad \theta = 0. \tag{7b}$$

The basic flow and temperature and pressure fields, whose stability forms the subject of this paper, are unaffected by the presence of inertia and are given by,

$$u = v = w = \psi = 0, \qquad \theta = 1 - y, \qquad p_y = R(1 - y). \tag{8}$$

3. Stability of the basic flow and weakly nonlinear solutions

We consider the stability of the solution given by (8) by means of a weakly nonlinear analysis similar in style to that of Newell and Whitehead (1969). Concentrating in the first instance on two–dimensional flows we shall determine those weakly nonlinear steady state solutions whose stability we shall consider in subsequent sections. Thus we assume that the Darcy–Rayleigh number is within $O(\epsilon^2)$ of its critical value (which is determined below), and expand the solution to (6) in a power series in ϵ:

$$\begin{pmatrix}\psi\\ \theta\end{pmatrix} = \epsilon\begin{pmatrix}\psi_1\\ \theta_1\end{pmatrix} + \epsilon^2\begin{pmatrix}\psi_2\\ \theta_2\end{pmatrix} + \epsilon^3\begin{pmatrix}\psi_3\\ \theta_3\end{pmatrix} + \dots, \tag{9}$$

and

$$R = R_0 + R_2\epsilon^2 + \dots. \tag{10}$$

As the presence of inertia is manifested as a nonlinear term it does not affect the linear stability analysis of the basic profile. In addition, we shall assume that the inertia parameter, G, is small and given by

$$G = G^*\epsilon. \tag{11}$$

It should be noted that equations (10) and (11) do not imply that the inertia parameter is a function of the deviation of R from its critical value. Rather,

we are assuming that G is very small, $O(\epsilon)$, and that the appropriate range of values of $R - R_c$ to consider is of magnitude $O(\epsilon^2)$. This allows us to consider the detailed transition between inertia–free and inertia–dominated flow.

At $O(\epsilon)$ we obtain the equations,

$$\nabla^2\psi_1 - R_0\theta_{1x} = 0, \tag{12a}$$

$$\nabla^2\theta_1 + \psi_{1x} = 0, \tag{12b}$$

for which the solutions are

$$\psi_1 = \Big(\frac{k^2+\pi^2}{k}\Big)A(\tau)\sin kx \sin \pi y, \tag{13a}$$

$$\theta_1 = A(\tau)\cos kx \sin \pi y, \tag{13b}$$

$$R_0 = \Big(\frac{k^2+\pi^2}{k}\Big)^2, \tag{13c}$$

where τ is a slow timescale given by $\tau = \frac{1}{2}\epsilon^2 t$. This solution corresponds to two–dimensional rolls with wavenumber, k. At $O(\epsilon^2)$ the solution is

$$\psi_2 = 0, \tag{14a}$$

$$\theta_2 = -A^2\Big(\frac{k^2+\pi^2}{8\pi}\Big)\sin 2\pi y, \tag{14b}$$

$$R_1 = 0, \tag{14c}$$

which is also identical to the Darcy–flow solution. At $O(\epsilon^3)$ a solution exists only if a solvability condition is satisfied; such a condition removes all components proportional to the $O(\epsilon)$ eigensolution from the inhomogeneous terms. This technique is now quite standard and we omit details of its application here. Application of the condition yields the following amplitude evolution equation for A:

$$A_\tau = \Big(\frac{2k^2}{k^2+\pi^2}\Big)R_2 A - \tfrac{4}{\pi}(k^2+\pi^2)^{5/2}I(k)G^*A|A| - \tfrac{1}{4}(k^2+\pi^2)^2A^3, \tag{15}$$

where

$$I(k) = (k^2+\pi^2)^{-3/2}\int_0^1\int_0^{2\pi/k}[k^2\cos^2 kx \sin^2 \pi y + \pi^2 \sin^2 kx \cos^2 \pi y]^{3/2}\,dx\,dy. \tag{16}$$

A sketch of typical solution curves is given in Fig. 1. The presence of inertia, which arises due to the $A|A|$ term in (15), is most obviously seen in the behaviour of the $A \neq 0$ curves near $R_2 = 0$. For small values of R_2, A satisfies

$$|A| \sim \frac{K^2\pi R_2}{2(k^2+\pi^2)G^*I(k)}, \tag{17}$$

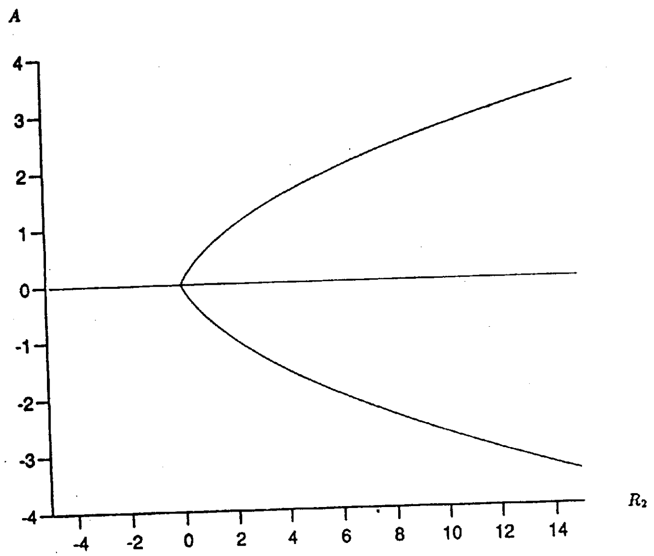

Fig. 1. A sketch of typical curves for weakly nonlinear convection in a porous medium in presence of fluid inertia; these curves are solutions of the equation $R_2A - A|A| - A^3 = 0$. The A-axis represents the zero solution which is stable when $R_2 < 0$ and unstable otherwise.

and therefore the solution curve has a finite slope near $R_2 = 0$, as opposed to the infinite slope which is characteristic of a standard pitchfork bifurcation. This behaviour was noted by He and Georgiadis, but since their analysis proceeded to second order their 'curve' was a straight line. Here, the third order analysis recovers the usual square–root dependence of A on R_2 for large values of R_2:

$$A^2 \sim \frac{8k^2 R_2}{(k^2 + \pi^2)^3}. \tag{18}$$

In the remainder of this paper we consider the weakly nonlinear flow at or very near to $k = \pi$, the wavenumber which minimises the critical Rayleigh number. Further, we shall rescale the amplitude by setting $A = A^*/\pi^2$; this has the effect of simplifying the coefficients of the amplitude equations when $k = \pi$, and we omit the asterisk superscript in the rescaled A.

4. The Eckhaus instability

This form of instability, also known as the sideband instability, is most readily analysed using a complex form of the above analysis. Bearing in mind that

$k = \pi$ and that the roll amplitude has now been rescaled, we begin the weakly nonlinear analysis by setting

$$\psi_1 = -(i/\pi)(Ae^{i\pi x} - \bar{A}e^{-i\pi x})\sin\pi y, \tag{19a}$$

$$\theta_1 = (1/\pi^2)(Ae^{i\pi x} + \bar{A}e^{-i\pi x})\sin\pi y, \tag{19b}$$

$$R_0 = 4\pi^2. \tag{19c}$$

The amplitude equation at $O(\epsilon^3)$ becomes

$$A_\tau = R_2 A + 4A_{XX} - \alpha A|A| - A^2\bar{A}, \tag{20}$$

where $A = A(X, \tau)$ and $X = \epsilon^2 x$ is a slow spatial variable which takes into account small, $O(\epsilon)$, deviations of the wavenumber from π. In equation (20) α is defined to be equal to $8\pi^2 IG^*$ where

$$I = I(\pi) = \int_0^1 \int_0^2 [\cos^2 kx \sin^2 \pi y + \sin^2 kx \cos^2 \pi y]^{3/2}\, dx\, dy = 0.776534. \tag{21}$$

This value for I has been computed using a two–dimensional trapezoidal rule and Richardson extrapolation, and is correct to six decimal places. We shall be considering the stability of steady roll solutions of wavenumber, $\pi + \epsilon K$, that is, solutions for which

$$A = A_0 e^{iKX} \qquad \text{where} \qquad A_0 = \frac{\pm 2(R_2 - 4K^2)}{[\alpha^2 + 4(R_2 - 4K^2)]^{1/2} + \alpha}. \tag{22}$$

Note that we shall always consider the positive value of A_0 in our analysis as exactly the same results are obtained for the negative value.

Sideband disturbances of infinitesimal amplitude are introduced by substituting

$$A = \left[A_0 + (\delta_1 e^{iLX} + \delta_2 e^{-iLX})e^{\lambda\tau}\right]e^{iKX} \tag{23}$$

into equation (20) and linearising the ensuing equations for δ_1 and δ_2. This results in the homogeneous system,

$$\begin{pmatrix} R_2 - 4(K+L)^2 - 2\alpha A_0 - 2A_0^2 - \lambda & -A_0^2 \\ -A_0^2 & R_2 - 4(K-L)^2 - 2\alpha A_0 - 2A_0^2 - \lambda \end{pmatrix}$$

$$\begin{pmatrix} \delta_1 \\ \delta_2 \end{pmatrix} = \begin{pmatrix} 0 \\ 0 \end{pmatrix}, \tag{24}$$

and therefore nonzero solutions exist only if the determinant of the matrix is zero. Hence the growth rate, λ, satisfies

$$\lambda = \pm(A_0^4 + 64L^2K^2)^{1/2} + R_2 - 4(K^2 + L^2) - 2\alpha A_0 - 2A_0^2. \tag{25}$$

On taking the positive sign in (25) to maximise the growth rate, setting $\lambda = 0$ to obtain neutrally stable modes, and noting that A_0 satisfies the equation

$$(R_2 - 4K^2)A_0 - \alpha A_0^2 - A_0^3 = 0, \tag{26}$$

equation (25) reduces to

$$A_0^2 + \alpha A_0 + 4L^2 = (A_0^4 + 64L^2K^2)^{1/2}. \tag{27}$$

The growth rate is also maximised over all values of L by setting $\frac{\partial\lambda}{\partial(L^2)} = 0$ in (25), and hence

$$8K^2 = (A_0^4 + 64L^2K^2)^{1/2}, \tag{28}$$

which can be rearranged to get

$$L^2 = K^2 - A_0^4/64K^2. \tag{29}$$

Equation (29) implies that sensible results can only be obtained when $A_0^2 \le 8K^2$ since then L^2 is positive. Substituting for L^2 from (29) into (27) yields

$$\alpha = \frac{(A_0^2 - 8K^2)^2}{16K^2 A_0}, \tag{30}$$

whilst using this value for α in (26) gives

$$R_2 = 8K^2 + A_0^4/16K^2. \tag{31}$$

When inertia is absent equations (27) and (29) can be solved explicitly (using A_0 given by (26)) to give the neutral curve, $R_2 = 12K^2$. When inertia is present we obtain the neutral curve by the following procedure: (i) choose a value of A_0, (ii) use (29) to obtain L^2, (iii) use (30) to obtain α, and (iv) use (31) to obtain R_2. The following table of values have been obtained using this procedure.

$\alpha/\lvert K\rvert$	$\lvert A_0/2K\rvert$	$\lvert L/K\rvert$	$R_2/4K^2$
0.00000	$2^{1/2}$	0.00000	3.00000
0.00057	1.4	0.19900	2.96040
0.03696	1.3	0.53477	2.71403
0.13067	1.2	0.69397	2.51840
0.50000	1.0	0.86603	2.25000
1.15600	0.8	0.94742	2.10240
2.24133	0.6	0.98367	2.03240
4.23200	0.4	0.99679	2.00640
9.60400	0.2	0.99980	2.00040
∞	0.0	1.00000	2.00000

Table 1. Neutral values of R_2 and L and the corresponding values of A_0 as a function of the inertia parameter, α.

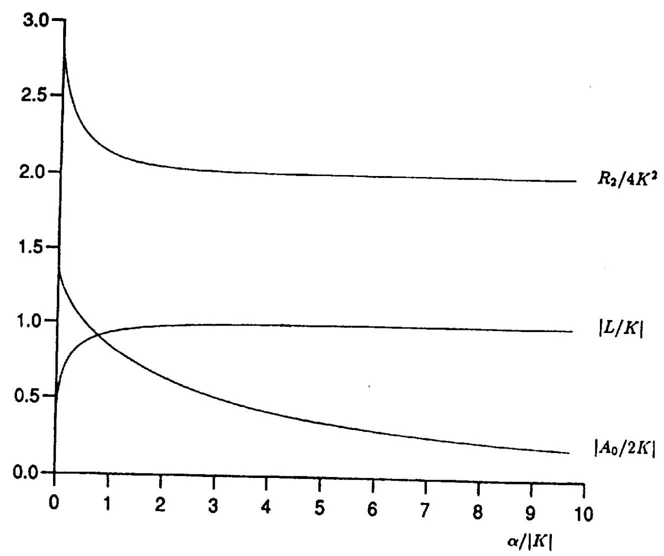

Fig. 2. Neutral values of R_2 and L and the corresponding values of A_0 as a function of the inertia parameter, α.

This numerical data is also shown in Fig. 2. It is interesting to note how quickly L rises from zero as α increases from zero, demonstrating that even a very weak presence of inertia has a profound effect on the preferred wavelength of the Eckhaus disturbances. In more detail, if we substitute $A_0 = 2\sqrt{2}K - \delta$ into equations (29), (30) and (31), where δ is assumed to be small and positive, we obtain

$$L \sim 2^{1/4}K^{1/2}\delta^{1/2}, \qquad \alpha \sim \delta^2/\sqrt{2}K \qquad \text{and} \qquad R_2 \sim 12K^2 - 4\sqrt{2}K\delta. \tag{32}$$

From this we find that $\alpha \sim L^4/2\sqrt{2}K^3$ when δ is sufficiently small. Thus L increases as the fourth root of α when α is small.

Thus we conclude that the presence of inertia serves to change substantially the wavelength of the most dangerous disturbance. The final column of the above table also indicates that the range of wavenumbers for which the basic flow is stable is larger than when inertia is absent, and is increasingly so as α increases: when $\alpha = 0$ we have $R_2 = 12K^2$ whereas when α is large, $R_2 \sim 8K^2$.

5. The zigzag instability

The form of instability is characterised by allowing the disturbances to have a weak three–dimensional dependence. Mathematically this is equivalent to a slow z–variation. Therefore the $O(\epsilon)$ temperature solution takes the form (19b) where

$$A = A(X, Z, \tau) \qquad \text{with} \qquad Z = \epsilon^{1/2} z. \tag{33}$$

As such a variation is three–dimensional, the streamfunction/temperature formulation used above has to be abandoned in favour of the primitive variables formulation given in (1). However, our previous experience (Rees and Riley (1989a)) indicates that the effect of a Z–dependence arises in such a way that there will be no coupling between it and the effect of inertia until that stage in the analysis where the amplitude equation is derived. Therefore we shall omit all reference to the details of the derivation and simply quote the amplitude equation:

$$A_\tau = R_2 A + \left(2\frac{\partial}{\partial X} - \frac{i}{\pi}\frac{\partial^2}{\partial Z^2}\right)^2 A - \alpha A|A| - A^2\bar{A}. \tag{34}$$

We perturb about the basic flow by setting,

$$A = \left[A_0 + (\delta_1 e^{i(LX+MZ\sqrt{\pi})} + \delta_2 e^{-i(LX+MZ\sqrt{\pi})})e^{\lambda\tau}\right]e^{iKX}. \tag{35}$$

Following the same procedure as in the last section we obtain the following expression for the growth rate, λ,

$$\lambda = \pm\left(A_0^4 + 64L^2(K+M^2)^2\right)^{1/2} + R_2 - 4((K+M^2)^2 + L^2) - 2\alpha A_0 - 2A_0^2 \tag{36}$$

which we maximise with respect to both L and M. One possibility is when $M = 0$, in which case we recover the Eckhaus instability. The other is when $K = -M^2$, which implies that K must be negative for this mechanism to be operative. When $K = -M^2$ defines M, it is straightforward to show that

$$R_2 = 6K^2 + 4K^4/\alpha^2 \tag{37}$$

is the neutral curve.

In the absence of inertia ($\alpha = 0$) the standard $K < 0$ criterion for instability is recovered. The presence of inertia can now be seen to increase the range of stable wavenumbers into the region where K is negative. One ramification of this is that under some circumstances for negative K it is possible that the Eckhaus disturbances grow while zigzag disturbances decay. It is easily verified that the two mechanisms are both neutral when

$$K = -(2-\sqrt{2})^{1/2}\alpha, \tag{38}$$

at which point

$$R_2 = (36 - 22\sqrt{2})K^2\alpha^2, \quad A_0 = -2(2-\sqrt{2})K\alpha \quad \text{and} \quad L = (5\sqrt{2} - 6)K\alpha/2. \tag{39}$$

Here the value of L refers to the Eckhaus disturbance wavenumber. Fig. 3 shows neutral curves corresponding to both instability mechanisms — we have chosen to set $\alpha = (2-\sqrt{2})^{-1/2}$ so that the transition between the two mechanisms takes place at $K = -1$.

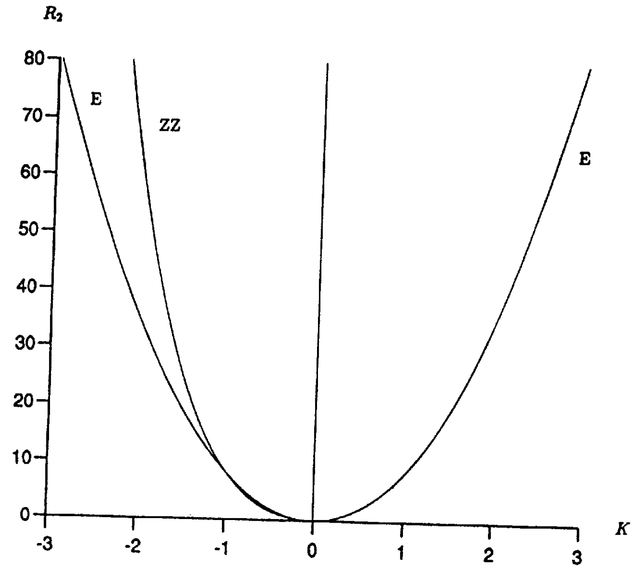

Fig. 3. Neutral curves for the Eckhaus and zigzag instabilities. The basic roll solution is unstable at points above the respective curves. Here $\alpha = (2-\sqrt{2})^{-1/2}$ so both types of disturbance are neutrally stable at the same value of R_2 when $K = -1$. 'E' denotes the Eckhaus instability and 'ZZ' the zigzag instability.

6. Cross–roll instability

In this section we consider the stability of rolls to disturbances of the form of rolls with other axial orientations. Such an analysis is necessarily three–dimensional and therefore we expand the solutions to equations (1) in powers of ϵ. At first order we superimpose two roll solutions with relative orientation, ϕ, by setting

$$p_1 = -(2/\pi)[A\cos\pi x + B\cos\pi(x\cos\phi - z\sin\phi)]\cos\pi y, \tag{40a}$$

$$\theta_1 = (1/\pi^2)[A\cos\pi x + B\cos\pi(x\cos\phi - z\sin\phi)]\sin\pi y, \tag{40b}$$

$$u_1 = -2[A\sin\pi x + B\cos\phi\sin\pi(x\cos\phi - z\sin\phi)]\cos\pi y, \tag{40c}$$

$$v_1 = 2[A\cos\pi x + B\cos\pi(x\cos\phi - z\sin\phi)]\sin\pi y, \tag{40d}$$

$$w_1 = 2[B\sin\phi\cos\pi(x\cos\phi - z\sin\phi)]\cos\pi y. \tag{40e}$$

In general it is necessary to write these solutions in complex form, following the example of (19), in order to obtain amplitude equations which allow the analysis of small variations in wavenumber, but we have presented them in the above form for the sake of clarity.

The solutions at second order in ϵ are considerably more complicated than (40) and therefore they are omitted here. At third order a solvability condition has to be applied once more; in this case we obtain a pair of equations which govern the evolution of both $A(X,\tau)$ and $B(X_B,\tau)$, where $X_B = \epsilon(x\cos\phi - z\sin\phi)$. These amplitude equations take the form,

$$A_\tau = R_2 A + 4A_{XX} - \alpha J_1(A,B,\phi) - A^2\bar{A} - \Omega(\phi)AB\bar{B}, \tag{41a}$$

$$B_\tau = R_2 B + 4B_{X_B X_B} - \alpha J_2(A,B,\phi) - B^2\bar{B} - \Omega(\phi)BA\bar{A}, \tag{41b}$$

where the coupling coefficient, Ω, which was derived in Rees and Riley (1989a), is given by

$$\Omega(\phi) = \frac{70 + 28\cos^2\phi - 2\cos^4\phi}{49 - 2\cos^2\phi + \cos^4\phi}. \tag{42}$$

The integrals, J_1 and J_2, are given by

$$J_1(A,B,\phi) = \frac{\sin\phi}{2I(\pi)}\int_0^2\int_0^1\int_0^{2/\sin\phi} q_1(u_1u_1^A + v_1v_1^A + w_1w_1^A)\,dz\,dy\,dx, \tag{43a}$$

and

$$J_2(A,B,\phi) = \frac{\sin\phi}{2I(\pi)}\int_0^2\int_0^1\int_0^{2/\sin\phi} q_1(u_1u_1^B + v_1v_1^B + w_1w_1^B)\,dz\,dy\,dx, \tag{43b}$$

and it should be noted that $J_1(A,B,\phi) = J_2(B,A,\phi)$. In (43) the superscripts, A and B, refer respectively to the terms multiplying A and B in equations (40c) to (40e). When $B = 0$ these integrals reduce to

$$J_1(A,0,\phi) = A|A| \quad \text{and} \quad J_2(A,0,\phi) = 0. \tag{44}$$

In (43) we set $q_1 = +(u_1^2 + v_1^2 + w_1^2)^{1/2}$.

We shall consider the stability of the roll solution, $A = A_0e^{iKX}$, $B = 0$, but now the disturbances take the form of inclined rolls. On setting $A = A_0e^{iKX} + \delta A$ and $B = \delta B$ into equations (41) and linearising, we find that the equations for δA and δB decouple. The equation for δA always yields decaying solutions but δB satisfies

$$\delta B_\tau = \left[R_2 - \Omega(\phi)A_0^2 - \alpha\frac{\partial J_2}{\partial B}\Big|_{B=0}\right]\delta B \tag{45a}$$

We note that

$$\frac{\partial J_2}{\partial B}\Big|_{B=0} = 1.1862|A_0| \equiv \beta|A_0|; \tag{45b}$$

this expression was obtained by means of a numerical differentiation of the integral (43b) and it defines the value of β. Thus neutrally stable modes occur when

$$R_2 = \alpha\beta A_0 + \Omega(\phi)A_0^2, \tag{46}$$

where it is assumed that A_0 is positive here, and therefore if A_0 is eliminated between (26) and (46), it is possible to find an explicit expression for the critical value of R_2 above which disturbances decay:

$$R_2 = \frac{\alpha(\Omega-\beta)\left[\left[\alpha^2(\beta-1)^2 + 16K^2(\Omega-1)\right]^{1/2} - \alpha(\beta-1)\right] + 8K^2\Omega(\Omega-1)}{2(\Omega-1)^2}. \tag{47}$$

A straightforward sketch of R_2 against A_0 using both (26) and (46) is sufficient to demonstrate that $\phi = 90^o$ provides the most restricted region of stability, since this value of ϕ minimises Ω, and therefore we shall concentrate on this case only. Before presenting plots of neutral curves it is instructive to consider the form of the cross–roll curves for both large and small values of K. When K is large R_2 takes the form,

$$R_2 \sim \frac{4\Omega K^2}{\Omega-1} + \frac{2\alpha(\Omega-\beta)K}{(\Omega-1)^{3/2}} = 40K^2/3 + 1.7277\alpha K, \tag{48}$$

where the first term is precisely the value obtained in the absence of inertia, and the second term, a positive value, indicates that this instability has a narrower range of stable wavenumbers when inertia is present. Equation (48) also applies in the limit of small values of α for fixed values of K. When K is small,

$$R_2 \sim \frac{4\beta K^2}{\beta-1} = 25.482K^2, \tag{49}$$

a result which is also more restrictive than the zero inertia case, and perhaps more importantly, than the Eckhaus instability (see Table 1) and the zigzag instability (see (37)) in the presence of inertia. Somewhat surprisingly this latter criterion is seemingly independent of α and would therefore suggest that it is also true for $\alpha = 0$. This conclusion is false, for the precise limiting expressions depend on the relative sizes of α and K. If $K \gg \alpha$ as $K \to 0$ then (48) is obtained, and if $\alpha \gg K$ as $\alpha \to 0$ then (49) is obtained. Intermediate values are obtained if K/α tends to a nonzero constant as both K and α tend to zero.

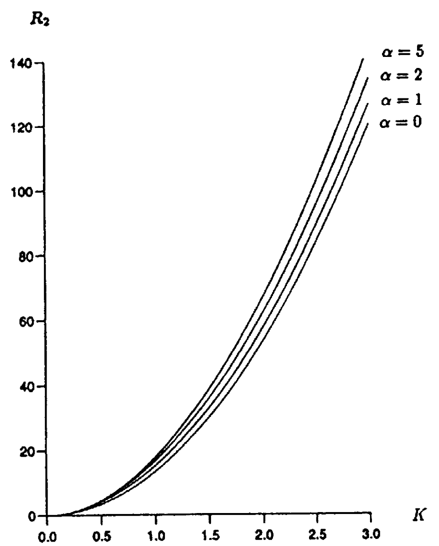

Fig. 4. Cross–roll instability neutral curves for various values of α.

In Fig. 4 we show cross–roll neutral curves to show how they vary with α. It may be seen that the region of stability decreases in size as α increases. In a fully three dimensional context the cross–roll instability curve always lies within the stable region determined by the Eckhaus analysis, but this is not true for the zigzag instability. A typical plot of neutral curves corresponding to all three instability mechanisms is given in Fig. 5. Clearly, for any nonzero value of α there is always a value of K for which the most dangerous cross–roll and zigzag disturbances are both neutrally stable. Mathematically, this point is determined by equating those values of R_2 given by (37) and (47), but K cannot be found in closed form. However, the use of simple Newton–Raphson algorithm has shown that this transition point is given by

$$K \simeq -1.4547\alpha \qquad \text{and} \qquad R_2 \simeq 30.608\alpha^2. \tag{50}$$

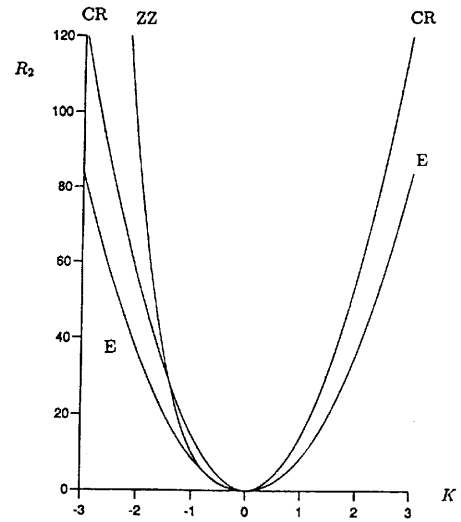

Fig. 5. A typical example of stability curves for all three instability mechanisms. These curves correspond to $\alpha = 1$. 'E' denotes the Eckhaus instability, 'ZZ' the zigzag instability, and 'CR' the cross–roll instability.

7. Conclusion

In this paper we have sought to determine how fluid inertia in the form of the Forchheimer terms modifies the weakly nonlinear stability of cellular convection in a porous layer heated from below. This analysis has considered the three common forms of instability mechanism known to operate in this type of flow: the Eckhaus, zigzag and cross–roll instabilities. The Eckhaus instability was found always to be less important than the cross–roll instability, but should the flow be constrained to be two–dimensional by virtue of the geometry of the layer, then we have shown that the range of stable wavenumbers increases in size as the inertia parameter, α, increases. When the flow is unrestricted in the third dimension the zigzag and cross–roll instabilities define the stability boundaries. We have found that the zigzag mechanism ceases always to destabilise flows with a wavenumber less than the critical value, thereby increasing the range of stable wavenumbers, but that the cross–roll instability is more restrictive.

Indeed, whenever $\alpha > 0$ there is always a range of negative values of K where cross–roll disturbances are more dangerous than the zigzag disturbances. All these observations serve to give both qualitative and quantitative predictions of the postcritical behaviour of Darcy–B'enard convection. Given the definition of the parameter, G^*, in equation (11), it is somewhat surprising that the strongest effects of inertia are felt when the flow is weakest. This means that it is not necessary, from a practical point of view, to attempt to produce high microscopic flow rates in order to validate or otherwise the quadratic inertia terms. Rather, we have found that the stability properties near to onset may be used for that purpose.

Acknowledgement. The author would like to thank Prof. H. I. Andersson for his very useful comments on the original manuscript.

References

ERGUN, S. 1952. Fluid flow through packed column, *Chem. Eng. Prog.*, **48**, 89-94.

FORCHHEIMER, P. 1901. Wasserbewegung durch boden, *Forschlft. Ver. D. Ingl.*, **45**, 1781-1788.

HASSANIZADEH, S.M. and GRAY, W.G. 1987. High velocity flow in porous media, *Transport in porous media*, **2**, 521-531.

HE, X.S. and GEORGIADIS J.G. 1990. Natural convection in porous media: effect of weak dispersion on bifurcation, *J. Fluid Mech.* **216**, 285-298.

HORTON, C.W. and ROGERS, F.T. 1945. Convection currents in a porous medium, *J. Appl. Phys.*, **16**, 367-370.

KVERNVOLD, O. and TYVAND, P.A. 1980. Dispersion effects on thermal convection in porous media, *J. Fluid Mech.*, **99**, 673-686.

LAPWOOD, E.R. 1948. Convection of a fluid in a porous medium, *Proc. Camb. Phil. Soc.*, **44**, 508-521.

MCKIBBIN, R. and O'SULLIVAN, M.J. 1980. Onset of convection in a layered porous medium heated from below, *J. Fluid Mech.*, **96**, 375-393.

MCKIBBIN, R. and O'SULLIVAN, M.J. 1981. Heat transfer in a layered porous medium heated from below, *J. Fluid Mech.*, **111**, 141-173.

NIELD, D.A. and JOSEPH, D.D. 1985. Effects of quadratic drag on convection in a saturated porous medium, *Phys. Fluids*, **28**, 995-997.

NEWELL, A.C. and WHITEHEAD, J.A. 1969. Finite bandwidth, finite amplitude convection, *J. Fluid Mech.*, **38**, 279-303.

RASOLOARIJAONA, M. and AURIAULT, J.L. 1994. Nonlinear seepage flow through a rigid porous medium, *European Journal of Mechanics B: Fluids*, **13**, 177-195.

REES, D.A.S. 1990. The effect of long-wavelength thermal modulations on the onset of convection in an infinite porous layer heated from below, *Q. J. Mech. Appl. Math.*, **43**, 189-214.

REES, D.A.S. and RILEY, D.S. 1989a. The effects of boundary imperfections on convection in a saturated porous layer: non-resonant wavelength excitation, *Proc. Roy. Soc. Lond.*, **A421**, 303-339.

REES, D.A.S. and RILEY, D.S. 1989b. The effects of boundary imperfections on convection in a saturated porous layer: near–resonant wavelength excitation, *J. Fluid Mech.*, **199**, 133-154.

REES, D.A.S. and RILEY, D.S. 1990. The three–dimensional stability of finite–amplitude convection in a layered porous medium heated from below, *J. Fluid Mech.*, **211**, 437-461.

RUTH, D. and MA, H. 1992. On the derivation of the Forchheimer equation by means of the averaging theorem, *Transport in Porous Media*, **7**, 255-264.

SCHLÜTER, A., LORTZ, D. and BUSSE, F.H. 1965. On the stability of finite–amplitude convection, *J. Fluid Mech.*, **23**, 129-144.